Biological and physical drivers of bio-mediated sediment resuspension: A flume study on Cerastoderma edule

Francesco Cozzoli, Tatiana Gomes da Conceição, Jeroen van Dalen, Xiaoyu Fang, Vojsava Gjoni, Peter M.J. Herman, Zhan Hu, Laura Soissons, Brenda Walles, Tom Ysebaert, et al.

Journal Pre-proof

Biological and physical drivers of bio-mediated sediment resuspension: A flume study on *Cerastoderma edule*

Francesco Cozzoli, Tatiana Gomes da Conceição, Jeroen Van Dalen, Xiaoyu Fang, Vojsava Gjoni, Peter M.J. Herman, Zhan Hu, Laura M. Soissons, Brenda Walles, Tom Ysebaert, Tjeerd J. Bouma

Please cite this article as: Cozzoli, F., Gomes da Conceição, T., Van Dalen, J., Fang, X., Gjoni, V., Herman, P.M.J., Hu, Z., Soissons, L.M., Walles, B., Ysebaert, T., Bouma, T.J., Biological and physical drivers of bio-mediated sediment resuspension: A flume study on *Cerastoderma edule*, *Estuarine, Coastal and Shelf Science* (2020), doi: https://doi.org/10.1016/j.ecss.2020.106824.
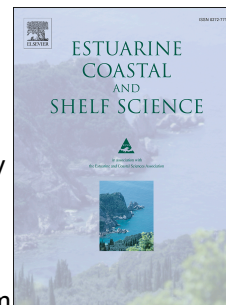
Francesco Cozzoli: Conceptualization, Data curation, Formal analysis, Investigation, Methodology, Resources, Software, Visualization, Writing -original draft.

Tatiana Gomes da Conceição: Conceptualization, Data curation, Formal analysis, Investigation, Methodology.

Jeroen Van Dalen: Conceptualization, Data curation, Formal analysis, Investigation, Methodology.

Xiaoyu Fang: Conceptualization, Writing - review & editing.

Vojsava Gjoni: Conceptualization, Writing - review & editing.

Zhan Hu: Writing - review & editing.

Laura M. Soissons: Writing - review & editing.

Brenda Walles: Writing - review & editing.

Peter M.J. Herman: Writing - review& editing,

Tom Ysebaert: Writing - review & editing.

Tjeerd J. Bouma: Conceptualization, Writing- review & editing, Funding acquisition, Project administration.

1 **Biological and physical drivers of bio-mediated sediment resuspension: a flume study**

2 **on *Cerastoderma edule***

3 Francesco Cozzoli[a,b,c,†], Tatiana Gomes da Conceição[b], Jeroen Van Dalen[b], Xiaoyu Fang[d],

4 Vojsava Gjoni[a], Peter M. J. Herman[e,f], Zhan Hu[g,h,§], Laura M. Soissons[b,i], Brenda Walles[j],

5 Tom Ysebaert[b,j], Tjeerd J. Bouma[b]

6 [a] Dipartimento di Scienze e Tecnologie Biologiche ed Ambientali, University of the Salento – 73100 Lecce,

7 Italy

8 [b] Department of Estuarine and Delta Systems. Royal Netherlands Institute of Sea Research (NIOZ) and Utrecht

9 University – 4401 NT Yerseke, The Netherlands

10 [c] Research Institute on Terrestrial Ecosystems (IRET) - National Research Council of Italy (CNR) via Salaria

11 km 29.3 – 00015 Monterotondo Scalo (Roma), Italy

12 [d] Marine Biology Research Group, Department of Biology, Ghent University – 9000 Ghent, Belgium

13 [e] Department of Hydraulic Engineering, Delft University of Technology – 2628 CN, P.O. Box 5048 2600 GA,

14 Delft, The Netherlands

15 [f] Deltares – P.O. Box 177 2600 MH, Delft, The Netherlands

16 [g] School of Marine Science, Sun Yat-sen University – 510275 Guangzhou, China

17 [h] Southern Laboratory of Ocean Science and Engineering (Guangdong, Zhuhai) – Zhuhai 519000, China

18 [i] MARBEC, Univ. Montpellier, CNRS, Ifremer, IRD – Sète, France

19 [j] Wageningen Marine Research, Wageningen University and Research – P.B. 77, 4400 AB Yerseke, The

20 Netherlands

21 [†]**Corresponding author**: Dipartimento di Scienze e Tecnologie Biologiche ed Ambientali.

22 Centro Ecotekne Pal. B S.P. 6 Lecce – Monteroni, 73100 Lecce, Italy;

23 francesco.cozzoli@unisalento.it

24 [§]**Corresponding author:** School of Marine Science, Sun Yat-sen University, 510275

25 Guangzhou, China; huzh9@mail.sysu.edu.cn.

26

27   **Abstract**

28   Predictive models accounting for the effect of bioturbation on sediment resuspension must be

29   based on ecological theory as well as on empirical parametrizations. The scaling trend of

30   individual metabolic and activity rates with body mass may be a key to the mechanistic

31   understanding of the observed patterns. With this study we tested if general size scaling rules

32   in bio-mediated sediment resuspension may apply to a broad range of physical contexts for

33   the endobenthic bivalve *Cerastoderma edule*. The effect on sediment resuspension of

34   populations of *C. edule* differing by individual size was measured across physical gradients of

35   current velocity and sediment composition in terms of fraction of fine particles. *C. edule* were

36   able to enhance the resuspension of sediment containing silt, while they had scarce effect on

37   the resuspension of coarse sediment. The effect of bioturbation was maximal at intermediate

38   current velocity, when the hydrodynamic forcing is not strong enough to overcome the abiotic

39   sediment resistance but it is able to suspend the bioturbated sediment. Although differences in

40   sediment silt content and intensities of hydrodynamic stress have a relevant influence in

41   determining the bioturbators individual contribution to sediment resuspension, the observed

42   mass scaling trend is consistent across all treatments and close to theoretical expectation for

43   size scaling of individual metabolic rates. This observation supports the hypothesis that the

44   contribution of individual bioturbators to sediment resuspension is directly related to their

45   energy use. Therefore, the proposed approach allows the formulation of expectations of biotic

46   contribution to sediment resuspension based on the general size scaling laws of individual

47   energy use.

48   *Keywords*: bioturbation; cohesiveness; body size; allometry; sediment resuspension;
49   *Cerastoderma edule*

50

1 Introduction

51

52 Sediment resuspension is mainly driven by the interaction between hydrodynamic forcing

53 and sediment particles (Le Hir, et al., 2000; Winterwerp & van Kesteren, 2004; Fagherazzi &

54 Wiberg, 2009; Zhou, et al., 2015), the outcome of which may be heavily modulated by biotic

55 agents (Le Hir, et al., 2007; Grabowski, et al., 2011; Friedrichs, 2011; Wilkes, et al., 2019).

56 In particular, the macrozoobenthic organisms disrupt and remix the sediment with their

57 moving, feeding and respiration activities in a process called bioturbation (Meysman, et al.,

58 2006; Kristensen, et al., 2012). Bioturbation alters the bottom sediment composition,

59 geochemistry and erodibility (Le Hir, et al., 2007; Sandford, 2008; Gogina, et al., 2018; Li, et

60 al., 2019). It happens at a local scale, but the effects may be important for broader landscape

61 processes (Widdows & Brinsley, 2002; Bentley Sr, et al., 2014; Walles, et al., 2015). The

62 bioturbators' ecosystem engineering [*sensu* (Jones, et al., 1994; Jones, et al., 1997)] of wet

63 sediment dynamics impacts the short- and long-term development of coastal geomorphology

64 (Winterwerp, et al., 2018; Gao, 2019), ecology (Zhu, et al., 2016; Lukwambe, et al., 2018;

65 Mermillod-Blondin, et al., 2018; Savelli, et al., 2019) and services provided to the human

66 society (Barbier, 2013; Bouma, et al., 2014; Lin, et al., 2018; Silva, et al., 2019). The role of

67 bioturbation should hence be taken into account in order to implement Ecosystem-Based

68 management of coastal areas (Braeckman, et al., 2014; Van der Biest, et al., 2020).

69 The large majority of flume experiments [*e.g.* (Widdows, et al., 1998; Willows, et al., 1998;

70 Orvain, et al., 2003; Kristensen, et al., 2013; Rakotomalala, et al., 2015; Cozzoli, et al.,

71 2019)], field observations [*e.g.* (Neumeier, et al., 2006; Montserrat, et al., 2008; Harris, et al.,

72 2015; Joensuu, et al., 2018; Hillman, et al., 2019)] and simulation studies [*e.g.* (Sandford,

73 2008; Orvain, et al., 2012; Nasermoaddeli, et al., 2018; Angeletti, et al., 2019)] agree that the

74 presence of bioturbators generally enhance sediment resuspension. However, bio-mediated

75 sediment dynamics often have complex non-linear behaviour (Balke, et al., 2012; Salvador

4

76 de Paiva, et al., 2018; Fang, et al., 2019; Xie, et al., 2019). For instance, some field

77 transplantation studies report tidal flat accretion in presence of high densities of the

78 bioturbator *Cerastoderma edule* (Andersen, et al., 2010; Donadi, et al., 2013), whereas flume

79 studies often show an increase in sediment resuspension.

80 Predictive models of bio-mediated physical dynamics should be based on generally valid

81 physicochemical and biological laws (van Prooijen, et al., 2011), able to encompass the broad

82 span of functional (Queirós, et al., 2013) and spatial (Gogina, et al., 2020) diversity observed

83 in nature. The individual size is a generally valid descriptor of the intensity of individual

84 bioturbation activity, with larger bioturbators having a higher bioturbation potential (Solan, et

85 al., 2004b; Gilbert, et al., 2007) and generating a greater increase in resuspension of bottom

86 sediment (Cozzoli, et al., 2018; Cozzoli, et al., 2019) and chlorophyll-a (Rakotomalala, et al.,

87 2015). This is because individual metabolic and activity rates increase with the individual

88 body mass following a power law with a scaling exponent of 0.66 or 0.75 (West, et al., 1997;

89 Kooijman, 2000; Vladimirova, et al., 2003; van der Meer, 2006; Hou, et al., 2008; Brey,

90 2010). A scaling exponent positive but lower than unity implies that, although the overall

91 individual metabolic rate increase with body mass, the metabolic rate per unit of mass

92 decrease with body mass with a scaling exponent of -0.33 or -0.25. The mass scaling of

93 metabolic rates is considered one of the most "universal" trends in ecology and it has

94 implications at any level of organization. Models based on the mass scaling of metabolic rates

95 can be used to predict general trends from individuals to ecosystems (Brown, et al., 2004;

96 Harris, et al., 2006; Martin, et al., 2013). In the case of bioturbation, the allometric scaling of

97 metabolic rates implies that larger individuals, having stronger respiration, feeding, burrowing

98 and moving activity, generate larger mechanical disturbance and hence weaken a larger

99 volume of the surrounding sediment. However, smaller individuals should have a larger effect

100 per unit of body mass because of their higher mass specific metabolic rate. Metabolic scaling

101 of bioturbation potential highlights the importance of the size structure of bioturbator

102 communities in determining the bioturbator influence on sediment characteristics (Cozzoli, et

103 al., 2018; Wrede, et al., 2019). The relationship between bioturbators metabolic rates at

104 population level and bio-mediated effects on sediment resuspension are generally valid for a

105 range of hydrodynamics stress conditions and a range of taxonomic and functional diversity

106 of the bioturbators (Cozzoli, et al., 2019).

107 Not only the intrinsic characteristics of the bioturbators, but also the extrinsic environmental

108 context can generate variations in bio-mediated sediment resuspension. In particular, the

109 sediment composition in terms of particle size distribution strongly affects resistance to

110 erosion. Silty (particles diameters $< 63\ \mu m$) and sandy (particles diameters between $63\ \mu m$

111 and 2 mm) sediments have different physical - chemical properties: as opposed to sand, silt

112 particles develop an asymmetric electrical charge distribution on their surfaces. This exerts a

113 net attractive force between particles, called cohesion. Once the amount of fine particles

114 reaches a certain threshold (*ca.* 10%), cohesion forces confer plasticity and "stickiness" to the

115 whole sediment mass, making it less erodible (van Ledden, et al., 2004; Winterwerp & van

116 Kesteren, 2004). Erosion and resuspension of non-cohesive sediment occurs once the

117 hydrodynamic stress exceeds the threshold for particle motion. The drivers of cohesive

118 sediment resuspension are more complex and relate not only to particle size and

119 hydrodynamic stress but also to the sediment compaction and mineral composition (Hayter &

120 Mehta, 1986; Winterwerp & van Kesteren, 2004; van Prooijen & Winterwerp, 2010) and to

121 the presence of microphytobenthos, which glues together sediment grains by producing

122 extracellular polymeric substance and hence increases sediment resistance to erosion

123 (Sutherland & Grant, 1998). The resuspension of sediments with different levels of

124 cohesiveness may be differently influenced by the effect of bioturbation activity. For instance,

125 recent field observations (Harris, et al., 2015; Joensuu, et al., 2018; Bernard, et al., 2019;

6

126   Hillman, et al., 2019), flume studies (Li, et al., 2017; Soissons, et al., 2019) and sediment

127   transport models (Nasermoaddeli, et al., 2018) showed that bioturbators enhance the

128   resuspension of fine sediment but have limited influence on coarse sediment.

129   Physical and biological drivers of sediment resuspension may establish complex interactions,

130   the effect of which has not yet been fully understood. In particular, the relationship between

131   bioturbators individual mass and bio-mediated sediment resuspension has not yet been

132   investigated across a range of extrinsic environmental conditions such as the composition and

133   degree of cohesiveness of the bioturbated sediment. Whereas field observations can be used to

134   investigate the effect of benthic organisms on sediment resuspension [*e.g.* (Orvain, et al.,

135   2007; Andersen, et al., 2010; Ubertini, et al., 2012; Savelli, et al., 2019)], stochasticity and

136   covariance between explanatory variables in the natural environment hamper the mechanistic

137   understanding of the processes involved. Studies conducted over fully factorial experimental

138   designs (*i.e.* crossing all combinations of target sources of variation) under controlled

139   (mesocosm) conditions are needed to disentangle the role of the different intrinsic and

140   extrinsic drivers of bio-mediated sediment dynamics (Orvain, et al., 2006; van Prooijen, et al.,

141   2011). Therefore, we used recirculating annular flumes in controlled mesocosm conditions to

142   test the hypotheses that the effect of the bioturbators on sediment resuspension should reflect

143   the intrinsic scaling trends of individual metabolic and activity rates over a range of extrinsic

144   conditions in terms of hydrodynamic stress and sediment silt fraction.

7

2 Material and Methods

2.1 Experimental design

The principal idea of this experiment is to explore how sediment resuspension is influenced

by physical and biological drivers (Figure 1). Therefore, we used a mesocosm approach to

quantify the importance of these drivers under controlled conditions, excluding bioturbator

behavioural changes in response to other environmental cues [*e.g.* acidification (Yvon-

Durocher, et al., 2012; Ong, et al., 2017); temperature (Verdelhos, et al., 2015a); salinity

(Verdelhos, et al., 2015b); food availability (Maire, et al., 2006)]. By mixing different types

of natural sediments, we were able to obtain 4 different levels of sediment silt volume content

(0 %, 4 %, 10 % and 28 %, Table 1) ranging from sand to sandy mud (van Rijn, 2007).

Recirculating annular flumes were used to simulate the natural dynamic changes in current

velocity during the tidal flooding of a mudflat (from 5 to 30 cm sec^{-1} by steps of 5 cm sec^{-1},

each step lasting 20 minutes). Variations in sediment resuspension were approximated from

water turbidity. To better focus on the contribution of the individual bioturbation activity, we

kept the overall bioturbators biomass constant (19 g Ash Free Dry Weight m^{-2}) as we

simultaneously varied the body size and the density of the tested specimens. Four different

size classes of individuals were used (36, 93, 247 and 576 mg AFDW of individual body

mass, Table 2). We chose to use an intermediate overall biomass of *C. edule* to avoid

overlapping between individuals' areas of influence (Zwarts, et al., 1994; Willows, et al.,

1998; van Prooijen, et al., 2011; Cozzoli, et al., 2018) while still having a clear and detectable

effect on sediment resuspension. Following a factorial design, each experimental treatment (2

replicates) was representative of a unique combination of bioturbators' individual size and

sediment composition in terms of silt content, for a total of 32 experimental runs with

bioturbators, each of which always used homogeneously sized individuals. Each of the

experimental runs with bioturbators was associated to a control run using the same sediment

170 type and current velocity gradient but without bioturbators. Considering that 6 repeated

171 measurements were taken at different current velocity levels for each run, we collected a total

172 of 384 data points (192 observations from bioturbated runs + 192 observations from control

173 runs, Figure 1). A numbers of replicates per treatment higher than the 2 we used would have

174 possibly given greater reliability ad reproducibility to our analysis. However, the logistic

175 efforts necessary for empirical testing did not make it possible to collect other measures.

176 While the dataset we collected may be regarded as not being "optimal", it is one of the most

177 complete experimental datasets (to our knowledge) on biota-mediated sediment resuspension

178 that has been measured according to gradients of individual size, individuals' density,

179 hydrodynamic energy and sediment composition. The obtained dataset is available as

180 appendix of this study (Appendix A) and in the OSF repository at DOI

181 10.17605/OSF.IO/BCWFH.

182 *2.2 Model organisms*

183 In this experiment, we used as model organism the bivalve *Cerastoderma edule* (Linnaeus,

184 1758)*. C. edule* (common cockle) is a species of saltwater clam in the family of Cardiidae

185 which is widely distributed in waters off northern Europe as far north as Iceland and into

186 waters of western Africa as far south as Senegal (Boyden, 1971). The ribbed oval shells can

187 reach 6 cm across and are white, yellowish or brown in colour. *C. edule* is a key element of

188 estuarine food webs, consuming suspended organic matter and being a main source of food

189 for birds (Bijleveld, et al., 2016). It is harvested commercially and eaten in much of its range

190 (Boyden, 1971). According to the Oosterschelde (NL) observations presented in (Cozzoli, et

191 al., 2014), this species can reach a relatively large individual body mass (up to 600 mg Ash

192 Free Dry Weight; on average 177 mg AFDW $\pm$ 202 s.d.), high density (up to 457 Ind. m^{-2};on

193 average 94 Ind. m^{-2} $\pm$ 55 s.d.) and biomass (up to 84 g AFDW m^{-2}; on average 16 g AFDW

194 m^{-2} $\pm$ 20 s.d.). *C. edule* is commonly found in a large variety of sediments ranging from fine

9

195   mud to sand, with a preference for cohesive sediments (Cozzoli, et al., 2013). The thermal

196   optimum for *C. edule* activity is 20 - 23 °C, above which the activity of the animal decreases

197   due to thermal stress, until a 100% of mortality when exposed for 120 hours to 32 °C

198   (Verdelhos, et al., 2015a). The salinity optimum is around 20-25, with a tolerance range from

199   fully marine (35) to brackish (10-15) (Verdelhos, et al., 2015b). Ocean acidification,

200   especially if associated to warming, may have a detrimental effect on physiological

201   performances and fitness of *C. edule* (Ong, et al., 2017).

202   *C. edule* is a filter feeder and shallow endobenthic burrower. Its short siphons usually emerge

203   from the sediment surface (Flach, 1996). Field and laboratory observations showed that its

204   reworking of the sediment is mostly related to bio-deposition, vertical and horizontal

205   movements and valve adduction that destabilize the cohesive sediment, making it more

206   erodible [*e.g.* (Flach, 1996; Ciutat, et al., 2007; Montserrat, et al., 2009; Li, et al., 2017)]. By

207   doing so, bioturbation by *C. edule* also enhances the resuspension of organic material and

208   microphytobenthos (Ubertini, et al., 2012; Rakotomalala, et al., 2015). The feeding rate of *C.*

209   *edule* is not significantly affected by changes in current speed, at least between 5 and 35 cm

210   sec^{-1} (Widdows & Navarro, 2007). The material filtered out from the water column is

211   deposited in the form of faeces (digested organic material) and pseudofaeces (discarded

212   sediment). Loose mucus bound pseudofaeces have a lower erosion threshold (current velocity

213   of 15 cm sec^{-1}) compared to faecal pellets (25 cm sec^{-1}). At flows below these thresholds,

214   biodeposits generated from *C. edule* tend to sediment and accumulate on the bed (Widdows

215   & Navarro, 2007).

216   *C. edule* is an excellent model organism to study bioturbation effects with high potential for

217   generalization because: *i*) it adapts well to laboratory conditions; *ii*) it constitutes a

218   predominant portion of the bioturbators intertidal biomass (Kater, et al., 2006) on a broad

219   geographical scale (Boyden, 1971); *iii*) recent evidence showed that the effect of this species

220   on sediment resuspension is common to a broad range of bioturbators functional types

221   (Cozzoli, et al., 2018; Cozzoli, et al., 2019); *iv*) the physiology and energetic of *C. edule* has

222   been carefully investigated due to the relevance of this species as ecological indicator and bio-

223   accumulator of pollutants (Fernández-Tajes, et al., 2011) *v*) its commercial importance for

224   shell fisheries and clam digging (Boyden, 1971).

225   *2.3 Experimental devices*

226   The recirculating annular flumes we used are a variation of the design described by

227   (Widdows, et al., 1998). The annular channel has a surface of 157 cm^2 and an overall height

228   of 40 cm, of which the bottom 5 cm are filled with a pebbled bed to allow water drainage,

229   followed by 10 cm of consolidated sediment and 20 cm of filtered marine seawater (31.4 L).

230   The water motion is generated by a smooth disk rotating 3 cm below the water surface, which

231   is driven by a microprocessor-controlled engine. Technical drawings and pictures of the

232   annular flume can be found in Appendix B. An acoustic Doppler velocimetry probe was used

233   to calibrate water velocity as a function of engine rotation speed. Water turbidity is measured

234   using an optical backscatter sensor (OBS 3+, Campbell scientific) facing the water

235   perpendicularly to the current direction at a height of 10 cm from the sediment surface. The

236   effect of suspended sediment on light absorption was measured by the OBS sensors in

237   nephelometric turbidity units every 30 seconds and converted into suspended sediment

238   concentration (g L^{-1}) based on calibration by gravitometric analysis (Appendix B).

239   *2.4 Experimental procedures*

240   <u>Sediment preparation:</u> The sediment was collected in late winter 2015 at location Oesterdam

241   (51° 30' N 4°10' E, sandy sediment) and Zandkreek Dam (51°32'N 3°52'E, silty sediment)

242   in the Oosterschelde and carefully sieved over a 1 mm sieve to avoid the presence of large

243   particles (stones, shells, wooden pieces) and remove larger animals. Successively, the

244 sediment was covered with a thick black plastic film for at least two weeks and sieved again

245 to remove remaining residual fauna. For each type of sediment composition, a homogeneous

246 matrix was obtained by adding silty sediment to a sandy matrix until reaching the desired

247 level of silt. The sediment was mixed manually. During mixing and sequential silt addition,

248 the percentage of silt in the sediment mass was measured by using a Malvern Mastersizer

249 2000® particle size analyser. Following this procedure, we obtained 4 different types of

250 sediment compositions, with no (0%), low (4%), intermediate (10%) and high (28%) silt

251 volume fraction (Table 1). The so prepared wet sediment was put in the flumes, mixed to a

252 smooth mass and allowed to consolidate until creating a layer of 10 cm height with a smooth

253 surface. Excess water in the sediment was drained through the pebbled bed placed at the

254 bottom. After 96 h, the flumes were filled with 31.4 L of filtered seawater (height of the

255 water column 20 cm). To prevent damage to the freshly-consolidated sediment surface, a

256 sheet of bubble plastic was placed on top of it before gently spraying water into the flume.

257 Although the sediment bottoms we obtained by this procedure may slightly differ from the

258 natural ones in term of grain size distribution, compaction and porewater gradient (Porter, et

259 al., 2006), they offer a representation of the sediment cohesiveness gradient that may be

260 observed along a mudflat tidal transect (Cozzoli, et al., 2013).

261 *Collection and measurement of specimens:* C. edule specimens were collected at the

262 Oesterdam during spring 2015. The authorization for specimen collection was issued by the

263 competent authority Rijkswaterstaat. After collection, the specimens were allowed to

264 acclimate for two weeks in a mesocosm at 18 °C. During the acclimation period, the

265 specimens were kept in the same sediment used for the experiment. Four different shell

266 length classes (15, 20, 27 and 35 mm of shell diameter [± 0.5 mm measurement error]) were

267 selected to cover the *C. edule* size gradient commonly observed in nature (Table 2).

268 Individual sizes were expressed as individual body masses (*M*, mg Ash Free Dry Weight) and

269 were estimated from the length of the cockles' shells according to the length-mass

270 relationships provided from the Monitor Taskforce of the Royal Netherlands Institute for Sea

271 Research (NIOZ), Yerseke. The mortality during the experiment was low and the specimens

272 were released at the collection site at the end of the experiments.

273 *Specimens addition:* A total biomass of 3 g AFDW (corresponding to 19 g AFDW m^{-2}) of *C.*

274 *edule* specimens of four different size classes (Table 2) were evenly distributed over the

275 sediment surface and allowed to settle for 48 h. The choice of a longer time interval (48 h)

276 compared with the typical interval between erosion stress peaks (typically 12 or 24 h in a

277 tidal system) was necessary to give the animals the time to properly settle in the new

278 environment and recover from manipulation stress. Most of them were buried within a few

279 minutes after being placed in the flume and non-burrowing individuals were replaced. During

280 their presence in the flume, some specimens crawled on and below the sediment surface,

281 leaving evident tracks.

282 *Erosion runs:* To simulate the natural dynamic changes in current velocity during flood tide,

283 we increased the current velocity (V, cm sec^{-1}) from 5 to 30 cm sec^{-1} in steps of 5 cm sec^{-1},

284 each step lasting 20 minutes. According to (Roberts, et al., 2000) and using a constant

285 friction factor for the sediment surface of 0.002, the range of current velocity used should

286 correspond to a range of bottom shear stresses between 0.05 and 0.25 Pa for a flat bottom.

287 Biogenic bottom roughness may increase the friction factor in presence of bioturbators,

288 implying a damping of bottom shear stress (Friedrichs, 2011; Anta, et al., 2013).

289 Bioturbator and control treatments have been prepared and run simultaneously. Each

290 treatment (2 bioturbated runs + 2 control runs) was carried out on the same day. According to

291 the availability of experimental flumes and considering the long preparation time to obtain a

292 consolidated bottom, we took *ca.* 2 months to complete the experiment.

293 *2.5 Data Analysis*

13

294   In this study, we did not consider extremely high values of suspended sediment deriving by

295   general failures of the flume bed and consequent mass erosion (Mehta & Partheniades, 1982;

296   van Prooijen & Winterwerp, 2010), although such mass erosion happened in some

297   treatments. Therefore, the collected dataset was preliminary inspected and records of mass

298   erosion events were removed from the analysis. We also removed some records clearly

299   biased by optical disturbance to the OBS sensor.

300   To express sediment resuspension in spatial units, we converted the measured suspended

301   sediment concentration (SSC, g L^{-1}) to total mass of suspended sediment per unit of sediment

302   surface (R_{TOT}, g m^{-2}) as:

303
$$R_{TOT} = \frac{SSC * Volume}{Area} \qquad \text{Eq. 1}$$

304   where *Area* is the surface area of the experimental flumes (0.157 m^2) and *Volume* is the

305   amount of contained water (31.4 L). The development of sediment erosion at the increase of

306   current velocity in the experimental flumes was analysed by visual inspection of the erosion

307   curves. Following (Kristensen, et al., 2013), the erosion thresholds, expressed as critical flow

308   velocity for starting sediment resuspension (V, cm sec^{-1}) were estimated for each treatment as

309   the zero R_{TOT} intercept from a regression of R_{TOT} measured at the end of each velocity step

310   (*i.e.* average R_{TOT} recorded during of the last two minutes of each current velocity step)

311   against *V*. Only measurements above the erosion threshold were used for this calculation.

312   The amount of suspended sediment due to bioturbation R_{BIO} (g m^{-2}) was calculated for each

313   replicate as:

314
$$R_{BIO} = R_{TOT\,(Bioturbated)} - R_{TOT\,(Control)} \qquad \text{Eq. 2}$$

14

315   where $R_{TOT_{(Bioturbated)}}$ (g m^{-2}) is the amount of sediment suspended at the end of each

316   current velocity step in the bioturbated treatment and $R_{TOT_{(Control)}}$ (g m^{-2}) is the amount of

317   sediment suspended in the corresponding control treatment.

318   The variation in R_{BIO} across experimental treatments and increasing current velocity (V, cm

319   sec^{-1}) steps was analysed by linear mixed ANCOVA. The different types of sediment

320   composition in terms of silt fraction (*Silt*) were used as categorical explanatory variable. The

321   current velocity (V, cm sec^{-1}) and the individual mass of the bioturbators (M, mg AFDW)

322   were used as continuous explanatory variables. The response variable R_{BIO} and the

323   explanatory variable M were normalized *via* log transformation. A third degree polynomial

324   function of the explanatory variable V was used to account for asymmetric concavity in the

325   shape of relationship between current velocity and R_{BIO}:

326    $$\log(R_{BIO}) \sim \log(M) * (V + V^2 + V^3) * Silt \qquad \text{Eq. 3}$$

327   where the operator "*" indicates use of the individual variables and their interaction terms.

328   We included the experimental runs as random term in the ANCOVA to account for non-

329   independence of the observations. This allows to treat properly the effect of V, which is

330   affected by repeated measurements during each erosion run. Selection of predictive variables

331   and interaction terms was assessed by bi-directional stepwise elimination procedure. All

332   analyses were performed within the free software environment R (R Core Team, 2019) using

333   the package lme4 (Bates, et al., 2015) and lmerTest (Kuznetsova, et al., 2017).

15

334   **3 Results**

335   *3.1 Erosion curves*

336   General bottom failure and mass erosion occurred at some current velocities (V, cm sec^{-1}) (all

337   the bioturbated treatments above V of 20 cm sec^{-1} for the sediment with 4 % silt content), for

338   some replicates (one replicate each for the treatments with 10 % and 28% silt content and

339   individual body mass M of 36 mg AFDW) and for one entire treatment (silt content 10 % and

340    $M = 247$ mg AFDW). These observations were probably related to lack of consolidation of

341   the sediment in the experimental flumes and outranged the turbidity sensor detection range.

342   Therefore, they were not considered in the following analyses (Figure 2).

343   In the absence of bioturbation, the critical flow velocity for erosion varied from 13.6 cm sec^{-1}

344   for sediment with 28% of silt to 17.2 cm sec^{-1} for sediment with 8% of silt (Figure 2, Table

345   3). Sediments with 0 % and 4 % of silt content were the most erodible at the higher current

346   velocity (> 20 cm sec^{-1}), reaching a R_{TOT} value of 121 ± 27.18 (s. d.) g m^{-2} and 187 ± 115 g

347   m^{-2} at maximal V (30 cm sec^{-1}), respectively (Figure 2). As we realized during the

348   experiment, R_{TOT} values for the sediment with 0% silt content may be slightly overestimated

349   due to the presence of some unidentified kind of organic matter generating a small amount of

350   foam and light hampering at high current velocity. Although we washed the sediment several

351   times, we were not able to remove this effect. Mass erosion was observed in some not

352   bioturbated controls for the sediment with 4 % of silt content at V of 30 cm sec^{-1}. Sediments

353   with 10 % and 28 % of silt content had relatively low values of R_{TOT} (61 ± 59 g m^{-2} and $36 \pm$

354   74 g m^{-2}, respectively) even at water velocity of 30 cm sec^{-1} (Figure 2).

355   For bioturbated treatments with 0% of silt content, we observed a moderate increase in R_{TOT}

356   at intermediate V values only (15 - 25 cm sec^{-1}) for $M = 36$ mg AFDW and $M = 247$ mg

357   AFDW. In these two treatments we also observed a decrease in critical flow velocity for

358   erosion from 15.5 to 8.5 cm sec^{-1}. A moderate decrease in R_{TOT} at maximal V was observed in

16

359   the two other bioturbated treatments (M = 93 mg AFDW and M = 576 mg AFDW) (Figure

360   2). The presence of *C. edule* had the strongest effect on R_{TOT} in the treatments with 4 % of silt

361   content. In this case, the bioturbators generated a decrease in the critical flow velocity for

362   erosion from 15.2 to *ca.* 5 cm sec^{-1} (9 cm sec^{-1} in the treatment with M =576 mg AFDW,

363   Table 3). This led to a moderate increase of R_{TOT} already at V = 10 cm sec^{-1} (especially the

364   two smaller size classes) and a very strong increase at V between 10 and 20 cm sec^{-1}. The

365   presence of bioturbators triggered mass erosion at V = 25 cm sec^{-1} (Figure 2). *C. edule* had

366   also a strong effect on sediment resuspension at 10 % and 28 % of silt content, although

367   without trigging mass erosion. In the case of the bioturbated sediment with 10% of silt

368   content, the critical flow velocity for erosion decreased from 17.2 to 10-12 cm sec^{-1} (Table 3).

369   A consistent increase in R_{TOT} due to bioturbation activity was observed starting from V = 15

370   cm sec^{-1} and continuously increasing with V until a value of + 150 ± 16 g m^{-2} for the

371   treatment with M = 93 mg AFDW. Bioturbators did not affect the critical flow velocity for

372   erosion of the sediment with 28 % of silt content (ca. 12 cm sec^{-1}, Table 3). Above this

373   threshold the bioturbators enhanced the erosion flux, leading to a maximal increment in R_{TOT}

374   of + 153 ± 19 g m^{-2} for the treatment with M = 36 mg AFDW (Figure 2).

375   *3.2 Biotic contribution to sediment resuspension*

376   Following the logarithmic transformation, the negative values of mass of suspended sediment

377   due to bioturbation activity (R_{BIO}, g m^{-2}, Equation 2) were excluded from the analysis.

378   Negative values of R_{BIO} implies a decrease in sediment resuspension in presence of

379   bioturbators and were observed mostly in the sediment with 0% silt content. As a

380   consequence of this selection and of that one made previously to avoid observations biased

381   by optical disturbance to the sensor, the total number of R_{BIO} values included in the analysis

382   has dropped to 135 (Table 4). The full mixed ANCOVA model of the variation R_{BIO} using the

383   silt content of the sediment (*Silt*), the current velocity (V, cm sec^{-1}) and the individual mass of

17

384   the bioturbators (M, mg AFDW) as explanatory variables (Equation 3) was simplified by bi-

385   directional elimination stepwise procedure. Following this procedure, the square term of the

386   polynomial of V, the third order interaction terms and some of the second order interaction

387   terms were eliminated. The full model (i.e. prior to variables selection) is available as an

388   appendix (Appendix C). The fixed terms in the simplified ANCOVA model explains 76% of

389   the observed variance in R_{BIO}, while random variation among experimental runs was able to

390   explain the 8% only (Table 5).

391   The model has good performances in predicting R_{BIO} for sediment with silt content higher

392   than 0 %. Given the low influence of the bioturbators on the resuspension of the pure sandy

393   sediment (Figure 2), the model fails in predicting R_{BIO} for these treatments (Figure 3, Figure

394   4). R_{BIO} significantly ($p < 0.001$) increases with the increase of V independently from the

395   sediment silt content and the body mass of bioturbators (Table 5, Figure 3, Figure 4). The

396   significant ($p < 0.001$) and negative coefficient for V^3 implies a concave shape in the

397   relationship between R_{BIO} and V (Table 5, Figure 3). The concavity of the relationship varies

398   significantly ($p < 0.001$) across sediment silt contents, being maximal for the sandy sediment,

399   intermediate for sediments with 10% and 28% silt content and minimal for the sediment with

400   4 % of silt content (Table 5, Figure 3). However, the nearly linear relationship between V and

401   R_{BIO} estimated for the sediment with 4 % silt content is likely to be an experimental artefact

402   related to the lack of observations for bioturbated treatments at V higher than 20 cm sec^{-1}

403   (Figure 2). Independently of the intensity of V and with only marginal variation across types

404   of sediment composition ($p > 0.05$), R_{BIO} scales significantly ($p < 0.001$) and negatively

405   (scaling exponent = -0.42 ± 0.22) with M (Table 5, Figure 4).

18

4 Discussion

In our experiments we used a full factorial combination of physical (sediment composition, hydrodynamic stress) and biological (bioturbator size/density ratio) drivers of bio-mediated sediment resuspension to disentangle the specific importance of each component and reveal the effect of their interactions (Figure 1). Although sediment resuspension patterns change across sediment types, the intrinsic scaling to the individual mass of the bioturbators was independent of the extrinsic physical context.

4.1 Effect of hydrodynamic stress and sediment composition on bio-mediated sediment resuspension

In accordance with previous flumes (Li, et al., 2017; Soissons, et al., 2019) and field (Harris, et al., 2015; Joensuu, et al., 2018; Bernard, et al., 2019) observations, bioturbation had a limited influence on the resuspension of pure sandy sediment, whereas it had a strong influence on resuspension of silt-containing sediments, even if only a low amount of silt was present (4 % volume fraction). In the case of sandy sediment, increments in sediment resuspension can be related to the exposure of otherwise buried fine particles to the buoyant action of the water (Volkenborn, et al., 2009; van Prooijen, et al., 2011). In the case of cohesive sediment, the bioturbation disrupts the cohesiveness and compaction in the upper sediment layers, generating a fluff layer (Shimeta, et al., 2002; Orvain, et al., 2003; Orvain, 2005). The fluff layer is less resistant to erosion than the not-bioturbated sediment, so that bioturbation decreases the critical flow velocity for erosion and enhances the erosion fluxes of cohesive sediment. Therefore, *C. edule* changed the sediment response to hydrodynamic stress by making the otherwise erosion-resistant cohesive sediments as erodible as the non-cohesive ones. Above the threshold for cohesiveness (10 % silt fraction), the effects of bioturbation on sediment resuspension no longer increases with sediment silt content. These observations support what was recently predicted by a landscape-scale model of biota-

19

431   mediated sediment resuspension on the basis of field observations of suspended sediment

432   concentration: the resuspension of fine silt in the southern North Sea is very sensitive to the

433   occurrence of bioturbators, whereas coarser sediment particles are less affected

434   (Nasermoaddeli, et al., 2018).

435   Our results suggest that if the hydrodynamic forcing is limited, the contribution of

436   bioturbation on sediment resuspension is relatively low. As well, if the hydrodynamics are

437   strong enough (or the sediment resistance weak enough, as it is in the case of non-cohesive

438   sediment) to erode the non-bioturbated sediment, the relative contribution of bioturbators to

439   sediment resuspension decreases because the additional bioturbation is less relevant for

440   particle motion. Bioturbation effects are maximal at intermediate current velocity, when the

441   hydrodynamic forcing is not strong enough to overcome the abiotic sediment resistance (that

442   is enhanced by cohesiveness) but are able to suspend the bioturbated sediment. This

443   interpretation is in line with the observations of (Moore, 2006), who noted that ecosystem

444   engineering in river morphodynamics can be more important with moderate hydrodynamic

445   energy and high bioturbators activity. Tending to be zero at very high and very low current

446   velocities for each type of sediment, the amount of suspended sediment due to bioturbation

447   activity has *per se* only marginally significant changes across sediment types. Neither is

448   changing its linear relationship with the current velocity. What actually changes across the

449   types of sediment is the current velocity at which bioturbators peak their effect on

450   resuspension. In sandy sediments, the bioturbators have a maximal effect at current velocity

451   of 20 cm sec^{-1}, above which the hydrodynamic stress starts to be able to suspend the non-

452   bioturbated sediment. Assuming a concave shape for the relationship between current velocity

453   and bioturbators contribution to sediment resuspension (Equation 3, Table 5), the maximal

454   effect on cohesive sediment resuspension should occur at a current velocity of *ca.* 40 cm sec^{-1}.

455   It also follows that the current velocity at which the bioturbators no longer have an

456   appreciable effect on the resuspension (*i.e* < 1 g m^{-2}) of the sediment is greater for the

457   cohesive sediment (*ca.* 60 cm sec^{-1}) than for the non-cohesive (*ca.* 40 cm sec^{-1}). It must be

458   however considered that our observations concern supply-limited erosion only (Mehta &

459   Partheniades, 1982; van Prooijen & Winterwerp, 2010). At current velocity higher than the

460   maximal we tested or in presence of waves, mass erosion (that may be triggered or anticipated

461   by the presence of bioturbators, as we observed in the treatments with 4 % of silt content)

462   may deviate from our expectations.

463   *4.2 Allometric scaling of individual contribution to sediment resuspension*

464   Given a fixed biomass, the contribution of a population of bioturbators to sediment

465   resuspension decrease with the bioturbators individual size. The estimated mass scaling

466   exponent (-0.42 ± 0.22) is different from either 0 (*i.e.* bio-mediated sediment resuspension

467   directly proportional to the population biomass) and -1 (*i.e.* bio-mediated sediment

468   resuspension directly proportional to the individuals' density in the case of biomass

469   equivalence across size classes). It is instead close to the theoretical expectations of -0.33 or -

470   0.25 for size scaling of individual metabolic rates per unit of biomass. In this respect, our

471   observations support the hypothesis that the contribution of bioturbators to sediment

472   resuspension is related to their metabolic and activity rate, rather than to their mere presence,

473   biovolume or spatial density (Cozzoli, et al., 2018; Cozzoli, et al., 2019). Therefore, a certain

474   biomass of smaller organism would generate a stronger disturbance of the sediment than the

475   same biomass of larger organisms because smaller organisms have higher metabolic rates per

476   unit of body mass. It follows that information on the size structure of the bioturbating

477   communities [*e.g.* (Gjoni, et al., 2017; Gjoni & Basset, 2018)] and on the individual

478   metabolic responses to internal and external conditions [*e.g.* (Rosenfeld, et al., 2015; Shokri,

479   et al., 2019)] is needed to predict the bioturbation effects on sediment resuspension.

480   Extrapolations based on bioturbators' overall biomass or density should instead be treated

21

481   with caution, because they may estimate wrongly the contribution of individuals differing by

482   body mass and activity level.

483   Although differences in sediment silt content and intensities of hydrodynamic stress have a

484   relevant influence in determining the bioturbators' individual contribution to sediment

485   resuspension, the observed mass scaling trend is constant across all treatments. Therefore,

486   size allometries in bio-mediated sediment resuspension can be generally applied to different

487   sediment compositions as well as to different functional types of bioturbators (Cozzoli, et al.,

488   2018; Cozzoli, et al., 2019). This finding expands the possibility to simplify and generalize

489   the process-based modelling of bioturbators-sediment interactions [*sensu* (van Prooijen, et

490   al., 2011)] by establishing a link between the energetic of the organisms and their effect on

491   the surrounding environment (Humphries & McCann, 2014). As an example referred to field

492   conditions, the bioturbators size, overall biomass and community bioturbation activity

493   generally peak in the intermediate-high part of the mudflat, where the hydrodynamic energy

494   is moderate and the sediment has an intermediate to high silt fraction (Pearson & Rosenberg,

495   1978; Nilsson & Rosenberg, 2002), *i.e.* where bioturbators are also more effective in

496   enhancing sediment resuspension. Thus, our results confirm and strengthen the hypothesis

497   that bioturbators mostly enhance the erosion of the upper shore, potentially inducing a

498   downward shift of the tidal flat (Wood & Widdows, 2002; Orvain, et al., 2012). More

499   generally, distribution models of benthic populations in relation to hydrodynamic and

500   sediment characteristics can be used to produce spatially explicit estimates of the individual

501   mass, abundance and therefore the potential effect on sediment resuspension of bioturbators

502   in natural conditions.

503   *4.3 Mechanisms to be further investigated*

504   In this study we attribute the changes in turbidity to changes in sediment erodibility.

505 However, some other mechanisms involved in bio-mediated sediment resuspension must be

506 considered. *C. edule* filter particles that are suspended in the water column while feeding.

507 The clearance activity may affect the amount of turbidity measured in the water in

508 recirculating flumes, possibly leading to an underestimation of the effect of *C. edule*

509 bioturbation on erosion rate, compared to field settings. This underestimation can reach a

510 factor of 2 in the case of chlorophyll-a suspension (Rakotomalala, et al., 2015). Despite

511 deserving to be examined more carefully, three main arguments suggests that suspended

512 sediment filtration can generate only a minor bias on our observations. Firstly, the filtered

513 sediment is not retained in the body of the bioturbators, but it is rather quickly expelled in the

514 form of pseudofaeces, that are easily erodible and likable to be re-suspended immediately at

515 current velocity > 15 cm sec^{-1} (Widdows & Navarro, 2007), *i.e.* with a similar critical flow

516 velocity for erosion to cohesive not-bioturbated sediment. Still, part of the decrease in

517 suspended sediment at high current velocity that we observed in some treatments with non-

518 cohesive sediment could be related to increased sediment strength by pelletization (Briggs, et

519 al., 2015). Secondly, being both fuelled by the individual metabolic rate, the magnitude of the

520 physiological activities involved in sediment destabilization and of the individual clearance

521 rate increase with body mass (decrease per unit of mass) with a similar scaling exponent

522 (Smaal, et al., 1997), leading to a substantial process balance across size classes. Thirdly,

523 previous studies comparing multiple types of bioturbators in a similar experimental setup

524 (Cozzoli, et al., 2018; Cozzoli, et al., 2019) did not show relevant differences in the

525 resuspension of sediment in the presence of filter feeders (*e.g. C. edule*) or bottom-feeders

526 (*e.g. Arenicola marina*).

527 Another mechanism to be further investigated is the effect of the structural modification of

528 the bottom surface roughness by bioturbators, which can be generated both in autologous

529 (emerging shells) and allogenic (disruption of the sediment surface) way. Bio-mediated

23

530 increases in bottom roughness could shelter the sediment surface from shear flow (Friedrichs,

531 et al., 2009; Friedrichs, 2011; Anta, et al., 2013). In the case of cohesive sediment, increased

532 bottom roughness may generate a reduction in sediment resuspension when the

533 hydrodynamic forcing is low (shear stress < 10 cm sec^{-1}) and/or the bioturbators abundance

534 (Ciutat, et al., 2007) or activity (Cozzoli, et al., 2019) is higher than what used in this

535 experiment. The reduction in cohesive sediment resuspension is suppressed at higher

536 hydrodynamic stress by the opposite destabilizing effect (Cozzoli, et al., 2019). With the

537 current experiment we show that, in case on pure sandy sediment, the sheltering and

538 pelletization effects could be the predominant influence of bioturbators, leading to a minor

539 reduction in sand resuspension at high current stress (30 cm sec^{-1}), even at the relatively low

540 number of organisms we used.

541 It must also be considered that in our experiment the individual body mass was calculated

542 based on shell length. Given the approximately spherical shape of *C. edule,* the individual

543 mass scales with the shell length with an exponent close to 3 (actually, 2.8). Therefore, our

544 observation could be eventually interpreted as an inverse proportionality between shell length

545 and effect on sediment resuspension (2.8*-0.42 = -1.12), which further leads to other

546 influencing factors such as burial depth, destabilization sediments beyond the surface layer

547 and autogenous modification of the bottom roughness. This interpretation should be rejected

548 considering that: *i*) given the experimental design we used, an inverse proportionality to the

549 individual length should exclude any effect of the individuals numerical density or total

550 biomass, and this is contrasting with all previous knowledge *ii*) previous experiments

551 comparing bioturbators with different physical shapes and therefore different scaling

552 coefficient for the mass ~ length relationship and/or generating different morphological

553 alterations of the bottom surface and/or with different burying depth related to their body

554 length showed no significant change in bioturbation effect on sediment resuspension

555 (Cozzoli, et al., 2018; Cozzoli, et al., 2019).

556 Finally, factorial experiments accounting for the effect of temperature change on bio-

557 mediated sediment resuspension could offer a definitive confirmation of the dependence on

558 metabolism of bioturbator populations. Water temperature is indeed a key regulator of

559 metabolic rates in ectotherms such as macrozoobenthic bioturbators (Brown, et al., 2007).

560 Beyond the effect of variation in physical factors (Nguyen, et al., 2019) it is expected that the

561 biotic contribution to sediment resuspension should increase positively with temperature

562 similarly to the individual metabolic rates, *i.e.* according to a positive Boltzmann – Arrhenius

563 relationship (Brown, et al., 2007). Therefore, metabolic-based approaches may help

564 explaining global and seasonal variations in biotic influences on sediment dynamics (Cozzoli,

565 et al., 2018; Wrede, et al., 2018).

566

567   **5 Conclusion**

568   With this study, we quantified the role of major sources of abiotic and biotic variability in

569   enhancing sediment resuspension by highlighting the combined role of physical and

570   biological factors in determining sediment resuspension. We observed that differences in

571   sediment silt content and intensities of hydrodynamic stress have a major influence in

572   determining the final amount of suspended sediment. However, the observed mass scaling

573   trend of bioturbators' individual contribution to sediment resuspension is *i*) close to the size

574   scaling trend of individual metabolic rates and *ii*) constant at the variation of the

575   environmental conditions. In the light of these findings, the bioturbators can be seen as

576   energy transfer units that convert the chemical energy contained in the food web into kinetic

577   energy that is discharged onto the sediment. The observation of a mass scaling exponent

578   similar to that of mass specific individual metabolic rates suggests that a somehow constant

579   fraction of metabolic energy is discharged onto the sediment at individual level. While the

580   intensity of the energy flow is determined by the body size and energy requirement of the

581   bioturbators, its effect on sediment resuspension is mediated by the hydrodynamic stress and

582   the mechanical characteristics of the sediment itself.

583   The metabolic dependency of bio-mediated sediment dynamics that we describe places our

584   observations within the broader context of metabolic ecological theories [*e.g.* (Kooijman,

585   2000; Brown, et al., 2004; Glazier, 2005; Hou, et al., 2008)]. It establishes a connection

586   between ecosystem engineering and general models of organisms metabolic [*e.g.* (Yvon-

587   Durocher, et al., 2012)] and demographic [*e.g.* (Dossena, et al., 2012; Lindmark, et al., 2018;

588   Bryndum-Buchholz, et al., 2019; Jørgensen, et al., 2019)] responses to global environmental

589   changes. Hence, our observations supports the parametrization of general, predictive models

590   of bio-mediated sediment dynamics at local [*e.g* . (Aquino, et al., 2017; Winterwerp, et al.,

591   2018)], tidal transect [*e.g.* (Wood & Widdows, 2002; Orvain, et al., 2012)] and landscape [*e.g.*

592   (Nasermoaddeli, et al., 2018; Angeletti, et al., 2019)] scale. By doing so, they open a venue to

593   the formulation of general expectations about future scenarios of bio-mediated sediment

594   resuspension.

595 *Acknowledgments*

603   **References**

604   Andersen, T. J. et al., 2010. Erodibility of a mixed mudflat dominated by microphytobenthos

605   and Cerastoderma edule, East Frisian Wadden Sea, Germany. *Estuar. Coast. Mar.*

606   *Sci.,* Volume 87, pp. 197-206.

607   Angeletti, S., Pierini, J. O. & Cervellini, P. M., 2019. Suspended sediment contribution

608   resulting from bioturbation in intertidal sites of a SW Atlantic mesotidal estuary: data

609   analysis and numerical modelling. *Sci. Mar.,* 82(4), pp. 245-256.

610   Anta, J., Peña, E., Puertas, J. & Cea, L., 2013. A bedload transport equation for the

611   Cerastoderma edule cockle. *J. Mar. Sys.,* Volume 111, pp. 189-195.

612   Aquino, T. et al., 2017. A process-based model for bioturbation-induced mixing. *Sci. Rep.,*

613   7(1), p. 14287.

614   Balke, T. et al., 2012. Conditional outcome of ecosystem engineering: A case study on

615   tussocks of the salt marsh pioneer Spartina anglica. *Geomorphology,* Volume 153, pp.

616   232-238.

617   Barbier, E., 2013. Valuing ecosystem services for coastal wetland protection and restoration:

618   Progress and challenges. *Resources,* 2(3), pp. 213-230.

619   Bates, D., Maechler, M., Bolker, S. & Walker, S., 2015. Fitting linear mixed-effects models

620   using lme4. *J. Stat. Soft.,* Volume 67, pp. 1-48.

621   Bentley Sr, S. J., Swales, A., Pyenson, B. & Dawe, J., 2014. Sedimentation, bioturbation, and

622   sedimentary fabric evolution on a modern mesotidal mudflat: A multi-tracer study of

623   processes, rates, and scales. *Estuar. Coast. Mar. Sci.,* Volume 141, pp. 58-68.

624   Bernard, G. et al., 2019. Quantifying bioturbation across coastal seascapes: Habitat

625   characteristics modify effects of macrofaunal communities. *J. Sea Res.,* Volume 152,

626   p. 101766.

627   Bijleveld, A. I. et al., 2016. Understanding spatial distributions: negative density-dependence

628   in prey causes predators to trade-off prey quantity with quality. *Proc. R. Soc. B,*

629   Volume 283, p. 20151557.

630   Bouma, T. J. et al., 2014. Identifying knowledge gaps hampering application of intertidal

631   habitats in coastal protection: Opportunities & steps to take. *Coast. Eng.,* Volume 87,

632   pp. 147-157.

633   Boyden, C. R., 1971. A note on the nomenclature of two European cockles. *Zool. J. Linnean*

634   *Soc.,* Volume 50, pp. 307-310.

635   Braeckman, U. et al., 2014. Protecting the commons: the use of subtidal ecosystem engineers

636   in marine management. *Aquatic Conserv: Mar. Freshw. Ecosyst.,* Volume

637   10.1002/aqc.2448.

638   Brey, T., 2010. An empirical model for estimating aquatic invertebrate respiration. *Methods*

639   *Ecol. Evol.,* Volume 1, p. 92–101.

640   Briggs, K., Cartwright, G., Friedrichs, C. & Shivarudruppa, S., 2015. Biogenic effects on

641   cohesive sediment erodibility resulting from recurring seasonal hypoxia on the

642   Louisiana shelf. *Cont. Shelf Res.,* Volume 93, pp. 17-26.

643   Brown, J., Allen, A. & Gillooly, J., 2007. The metabolic theory of ecology and the role of

644   body size in marine and freshwater ecosystems. In: *Body size: the structure and*

645   *function of aquatic ecosystems.* Cambrige: Cambridge University Press, pp. 1-15.

646   Brown, J. et al., 2004. Toward a metabolic theory of Ecology. *Ecology,* Volume 82, p. 1771–

647   1789.

648   Bryndum-Buchholz, A. et al., 2019. Twenty-first-century climate change impacts on marine

649   animal biomass and ecosystem structure across ocean basins. *Global Change Biol.,*

650   25(2), pp. 459-472.

651 Ciutat, A., Widdows, J. & Pope, N. D., 2007. Effect of Cerastoderma edule density on near-

652   bed hydrodynamics and stability of cohesive muddy sediments. *J. Exp. Mar. Bio.*

653   *Ecol.,* 346(1–2), pp. 114-126.

654 Cozzoli, F. et al., 2018. The combined influence of body size and density on cohesive

655   sediment resuspension by bioturbators. *Sci. Rep.,* 12.8(3831).

656 Cozzoli, F., Bouma, T. J., Ysebaert, T. & Herman, P. M. J., 2013. Application of non-linear

657   quantile regression to macrozoobenthic species distribution modelling: Comparing

658   two contrasting basins. *Mar. Ecol. Prog. Ser.,* Volume 475, pp. 119-133.

659 Cozzoli, F. et al., 2014. A mixed modeling approach to predict the effect of environmental

660   modification on species distributions.. *PLoS One,* Volume 9, p. 15–17.

661 Cozzoli, F. et al., 2019. A process based model of cohesive sediment resuspension under

662   bioturbators' influence. *Sci. Tot. Env.,* Volume 670, pp. 18-30.

663 Donadi, S. et al., 2013. Cross-habitat interactions among bivalve species control community

664   structure on intertidal flats. *Ecology,* Volume 94, pp. 489-498.

665 Dossena, M. et al., 2012. Warming alters community size structure and ecosystem

666   functioning. *Proc. R. Soc. Lond. B. Biol. Sci.,* 279(1740), pp. 3011-3019.

667 Fagherazzi, S. & Wiberg, P. L., 2009. Importance of wind conditions, fetch, and water levels

668   on wave-generated shear stresses in shallow intertidal basins. *J. Geophys. Res.,*

669   Volume 114, p. F03022.

670 Fang, X. et al., 2019. Spatio-temporal variation in sediment ecosystem processes and roles of

671   key biota in the Scheldt estuary. *Estuar. Coast. Mar. Sci.,* Volume 222, pp. 21-31.

672 Fernández-Tajes, J. et al., 2011. Use of three bivalve species for biomonitoring a polluted

673   estuarine environment. *Environ. Monit. Assess.,* Volume 177, pp. 289-300.

674 Flach, E., 1996. The influence of the cockle, Cerastoderma edule, on the macrozoobenthic

675   community of tidal flats in the Wadden Sea. *Mar. Ecol. - PSZNI,* 17(I), pp. 87-98.

676 Friedrichs, C. T., 2011. Tidal Flat Morphodynamics. In: E. Wolanski & D. McLusky, red.

677   *Tidal Flat Morphodynamics.* sl:Elsevier, p. 4590.

678 Friedrichs, M., Leipe, T., Peine, F. & Graf, G., 2009. Impact of macrozoobenthic structures

679   on near-bed sediment fluxes. *J. Mar. Sys.,* Volume 75, p. 336–347.

680 Gao, S., 2019. Geomorphology and sedimentology of tidal flats. In: G. Perillo, E. Wolanski,

681   D. Cahoon & C. Hopkinson, red. *Coastal Wetlands.* sl:Elsevier Science, pp. 359-381.

682 Gilbert, F. et al., 2007. Sediment reworking by marine benthic species from the GullmarFjord

683   (Western Sweden): Importance of faunal biovolume. *J. Exp. Mar. Biol. Ecol.,* Volume

684   348, p. 133–144.

685 Gjoni, V. & Basset, A., 2018. A cross-community approach to energy pathways across lagoon

686   macroinvertebrate guilds. *Estuaries Coast.,* 41(8), pp. 2433-2446.

687 Gjoni, V., Cozzoli, F., Rosati, I. & Basset, A., 2017. Size–Density Relationships: a Cross-

688   Community approach to benthic macroinvertebrates in Mediterranean and Black Sea

689   Lagoons. *Estuaries Coast.,* 40(4).

690 Glazier, D. S., 2005. Beyond the '3/4-power law': variation in the intra- and interspecific

691   scaling of metabolic rate in animals. *Biol. Rev.,* Volume 80, pp. 611-662.

692 Gogina, M. et al., 2018. In search of a field-based relationship between benthic macrofauna

693   and biogeochemistry in a modern brackish coastal sea. *Front. Mar. Sci.,* 5(489).

694 Gogina, M. et al., 2020. Interregional comparison of benthic ecosystem functioning:

695   community bioturbation potential in four regions along the NE Atlantic shelf. *Ecol.*

696   *Ind.,* 110(105945).

697 Grabowski, R. C., Droppo, I. G. & Wharton, G., 2011. Erodibility of cohesive sediment: The

698   importance of sediment properties. *Earth-Sci. Rev.,* 105(3-4), pp. 101-120.

699 Harris, J. et al., 2015. Biotic interactions influence sediment erodibility on wave-exposed

700   sandflats. *Mar. Ecol. Prog. Ser.,* Volume 523, pp. 15-30.

701 Harris, J. et al., 2015. Biotic interactions influence sediment erodibility on wave-exposed
702   sandflats. *Mar. Ecol. Prog. Ser.,* Volume 523, pp. 15-30.

703 Harris, L. A., Duarte, C. M. & Nixon, S. W., 2006. Allometric laws and prediction in
704   estuarine and coastal ecology. *Estuaries Coast.,* 29(2).

705 Hayter, E. J. & Mehta, A. J., 1986. Modelling cohesive sediment transport in estuarial waters.
706   *Appl. Math. Model.,* Volume 10, pp. 294-303.

707 Hillman, J. R., Lundquist, C. J., Pilditch, C. A. & Thrush, S. F., 2019. The role of large
708   macrofauna in mediating sediment erodibility across sedimentary habitats. *Limnol.*
709   *Oceanogr.,* Volume doi:10.1002/lno.11337.

710 Hou, C. et al., 2008. Energy uptake and allocation during ontogeny. *Science ,* 322(5902), pp.
711   736-739.

712 Humphries, M. M. & McCann, K. S., 2014. Metabolic ecology. *J. Anim. Ecol.,* 83(1), pp. 7-
713   19.

714 Jørgensen, L. L. et al., 2019. Impact of multiple stressors on sea bed fauna in a warming
715   Arctic. *Mar. Ecol. Prog. Ser.,* Volume 608, pp. 1-12.

716 Joensuu, M. et al., 2018. Sediment properties, biota, and local habitat structure explain
717   variation in the erodibility of coastal sediments. *Limnol. Oceanogr.,* Volume 63, p.
718   173–186.

719 Jones, C. G., Lawton, J. H. & Shachak, M., 1994. Organisms as ecosystem engineers. *Oikos,*
720   Volume 69, pp. 373-386.

721 Jones, C. G., Lawton, J. H. & Shachak, M., 1997. Positive and negative effects of organisms
722   as physical ecosystem engineers. *Ecology,* Volume 78, pp. 1946-1957.

723 Kater, B., Geurts van Kessel, A. & Baars, J., 2006. Distribution of cockles cerastoderma edule
724   in the eastern scheldt: habitat mapping with abiotic variables. *Mar. Ecol. Prog. Ser.,*
725   Volume 318, pp. 221-227.

726   Kooijman, S. A. L. M., 2000. *Dynamic energy and mass budgets in biological systems.*

727   Cambridge: Cambridge University Press.

728   Kristensen, E. et al., 2013. Influence of benthic macroinvertebrates on the erodability of

729   estuarine cohesive sediments: Density- and biomass-specific responses. *Estuar. Coast.*

730   *Shelf Sci.,* Volume 134, pp. 80-87.

731   Kristensen, E. et al., 2012. What is bioturbation? The need for a precise definition for fauna in

732   aquatic sciences. *Mar. Ecol. Prog. Ser.,* Volume 446, pp. 285-302.

733   Kuznetsova, A., Brockhoff, P. B. & Christensen, R. H. B., 2017. lmerTest Package: Tests in

734   Linear Mixed Effects Models. *J. Stat. Soft.,* 82(13), pp. 1-26.

735   Le Hir, P., Monbet, Y. & Orvain, F., 2007. Sediment erodability in sediment transport

736   modelling: Can we account for biota effects?. *Conti. Shelf Res.,* Volume 27, pp. 1116-

737   1142.

738   Le Hir, P. et al., 2000. Characterization of intertidal flat hydrodynamics. *Cont. Shelf Res.,*

739   20(12-13), pp. 1433-1459.

740   Li, B. et al., 2019. Effects of key species mud snail Bullacta exarata (Gastropoda) on oxygen

741   and nutrient fluxes at the sediment-water interface in the Huanghe River Delta, China.

742   *Acta Oceanol. Sin.,* 38(8), pp. 48-55.

743   Li, B. et al., 2017. Bioturbation effect on the erodibility of cohesive versus non-cohesive

744   sediments along a current velocity gradient: a case study on cockles. *J. Exp. Mar. Biol.*

745   *Ecol.,* Volume 496, pp. 84-90.

746   Lin, D. et al., 2018. Bioturbation facilitates DDT sequestration by activated carbon against

747   recontamination by sediment deposition. *Environ. Toxicol. Chem.,* 37(7), pp. 2013-

748   2021.

749   Lindmark, M., Ohlberger, J., Huss, M. & Gårdmark, A., 2018. Size-based ecological

750   interactions drive food web responses to climate warming. *bioRxiv,* Volume 430082.

751   Lukwambe, B. et al., 2018. Bioturbation by the razor clam(Sinonovacula constricta) on the

752   microbial community and enzymatic activities in the sediment of an ecological

753   aquaculture wastewater treatment system. *Sci. Tot. Env.,* Volume 643, pp. 1098-1107.

754   Maire, O. et al., 2006. Effects of food availability on sediment reworking in Abra ovata and

755   A. nitida. *Mar. Ecol. Prog. Ser.,* Volume 319, pp. 135-153.

756   Martin, B. T. et al., 2013. Predicting population dynamics from the properties of individuals:

757   A cross-level test of dynamic energy budget theory. *Am. Nat.,* 181(4), pp. 506-519.

758   Mehta, A. & Partheniades, E., 1982. *Resuspension of deposited cohesive sediment beds.* Cape

759   Town, 18th Conference on Coastal Engineering ASCE.

760   Mermillod-Blondin, F. et al., 2018. Influence of tubificid worms on sediment structure,

761   benthic biofilm and fauna in wetlands: A field enclosure experiment. *Freshwater*

762   *Biol.,* 63(11), pp. 1420-1432.

763   Meysman, F. J., Middelburg, J. J. & Heip, C. H., 2006. Bioturbation: a fresh look at Darwin's

764   last idea. *Trend. Ecol. Evol.,* 21(12), pp. 688-695.

765   Montserrat, F. et al., 2008. Benthic community-mediated sediment dynamics. *Mar. Ecol.*

766   *Prog. Ser.,* Volume 372, pp. 43-59.

767   Montserrat, F. et al., 2009. Sediment segregation by biodiffusing bivalves. *Estuar. Coast.*

768   *Mar. Sci.,* 83(4), pp. 379-391.

769   Moore, J. W., 2006. Animal ecosystem engineers in streams. *BioScience,* Volume 56, pp.

770   237-246.

771   Nasermoaddeli, M. H. et al., 2018. A model study on the large-scale effect of macrofauna on

772   the suspended sediment concentration in a shallow shelf sea. *Estuar. Coast. Mar. Sci.,*

773   Volume 211, pp. 62-76.

774   Neumeier, U., Lucas, C. H. & Collins, M., 2006. Erodibility and erosion patterns of mudflat

775   sediments investigated using an annular flume. *Aquat. Ecol.,* Volume 40, pp. 543-554.

776   Nguyen, H. M., Bryan, K. R., Pilditch, C. A. & Moon, V. G., 2019. Influence of ambient

777   temperature on erosion properties of exposed cohesive sediment from an intertidal

778   mudflat.. *Geo Marine Lett.,* 39(4), pp. 337-347.

779   Nilsson, H. C. & Rosenberg, R., 2002. Succession in marine benthic habitats and fauna in

780   response to oxygen deficiency: analysed by sediment profile-imaging and by grab

781   samples. *Mar. Ecol. Prog. Ser.,* Volume 197, pp. 139-149.

782   Ong, E. Z., Briff, M., Moens, T. & Van Colen, C., 2017. Physiological responses to ocean

783   acidification and warming synergistically reduce condition of the common cockle

784   Cerastoderma edule. *Mar. Env. Res.,* Volume 130, pp. 38-47.

785   Orvain, F., 2005. A model of sediment transport under the influence of surface bioturbation:

786   generalisation to the facultative suspension-feeder Scrobicularia plana. *Mar. Ecol.*

787   *Prog. Ser.,* Volume 286, pp. 43-56.

788   Orvain, F., Le Hir, P. & Sauriau, P. G., 2003. A model of fluff layer erosion and subsequent

789   bed erosion in the presence of the bioturbator, Hydrobia ulvae. *J. Mar. Res.,* Volume

790   61, pp. 823-851.

791   Orvain, F., Le Hir, P., Sauriau, P. G. & S., L., 2012. Modelling the effects of macrofauna on

792   sediment transport and bed elevation: Application over a cross-shore mudflat profile

793   and model validation. *Estuar. Coast. Mar. Sci.,* Volume 108, pp. 64-75.

794   Orvain, F., Sauriau, P. G., Bacher, C. & Prineau, M., 2006. The influence of sediment

795   cohesiveness on bioturbation effects due to Hydrobia ulvae on the initial erosion of

796   intertidal sediments: a study combining flume and model approaches. *J. Sea Res. ,*

797   55(1), pp. 54-73.

798   Orvain, F. et al., 2007. Spatio-temporal variations in intertidal mudflat erodability: Marennes-

799   Oléron Bay, western France. *Cont. Shelf Res.,* 27(8), pp. 1153-1173.

800 Pearson, T. H. & Rosenberg, R., 1978. Macrobenthic succession in relation to organic

801   enrichment and pollution of the marine environment. *Oceanogr. Mar. Biol. Ann. Rev.,*

802   Volume 5, pp. 229-311.

803 Porter, E. T., Owens, M. S. & Cornwell, J. C., 2006. Effect of sediment manipulation on the

804   biogeochemistry of experimental sediment systems. *J. Coast. Res.,* 22(6), pp. 1539-

805   1551.

806 Queirós, A. M. et al., 2013. A bioturbation classification of E uropean marine infaunal

807   invertebrates. *Ecol. Evol.,* 3(11), pp. 3958-3985.

808 R Core Team, 2019. *R: A language and environment for statistical computing.* [Online]

809   Available at: https://www.R-project.org/

810 Rakotomalala, C. et al., 2015. Modelling the effect of Cerastoderma edule bioturbation on

811   microphytobenthos resuspension towards the planktonic food web of estuarine

812   ecosystem. *Ecol. Model.,* Volume 316, pp. 155-167.

813 Roberts, W., Le Hir, P. & Whitehouse, R., 2000. Investigation using simple mathematical

814   models of the effect of tidal currents and waves on the profile shape of intertidal

815   mudflats. *Cont. Shelf Res.,* 20(10-11), pp. 1079-1097.

816 Rosenfeld, J., Van Leeuwen, T., Richards, J. & Allen, D., 2015. Relationship between growth

817   and standard metabolic rate: measurement artefacts and implications for habitat use

818   and life-history adaptation in salmonids. *J. Anim. Ecol.,* 84(1), pp. 4-20.

819 Salvador de Paiva, J. N., Walles, B., Ysebaert, T. & Bouma, T. J., 2018. Understanding the

820   conditionality of ecosystem services: The effect of tidal flat morphology and oyster

821   reef characteristics on sediment stabilization by oyster reefs. *Ecol. Eng.,* Volume 112,

822   pp. 89-95.

823 Sandford, L. P., 2008. Modeling a dynamically varying mixed sediment bed with erosion,

824 deposition, bioturbation, consolidation, and armoring. *Comput. Geosci.,* Volume 34,

825 pp. 1263-1283.

826 Savelli, R. et al., 2019. Impact of chronic and massive resuspension mechanisms on the

827 microphytobenthos dynamics in a temperate intertidal mudflat. *J. Geophys. Res.*

828 *Biogeo.,* Volume 124.

829 Shimeta, J., Amos, C. L., Beaulieu, S. E. & Ashiru, O. M., 2002. Sequential resuspension of

830 protists by accelerating tidal flow: implications for community structure in the benthic

831 boundary layer. *Limnol. Oceanogr.,* 47(4), pp. 1152-1164.

832 Shokri, M. et al., 2019. Components of standard metabolic rate variability in three species of

833 gammarids. *Web Ecology,* 19(1), pp. 1-13.

834 Silva, R. et al., 2019. The incorporation of biophysical and social components in coastal

835 management. *Estuaries Coast.,* pp. 1-14.

836 Smaal, A. C., Vonck, A. P. M. A. & Bakker, M., 1997. Seasonal variation in physiological

837 energetics of Mytilus edulis and Cerastoderma edule of different size classes. *J. Mar.*

838 *Biol. Assoc. U. K.,* 77(3), pp. 817-838.

839 Soissons, L. M. et al., 2019. Sandification vs. muddification of tidal flats by benthic

840 ecosystem engineers: a flume study. *Estuar. Coast. Mar. Sci.,* Volume 228, p. 106355.

841 Solan, M. et al., 2004b. In situ quantification of bioturbation using time lapse fluorescent

842 sediment profile imaging (f SPI), luminophore tracers and model simulation. *Mar.*

843 *Ecol. Prog. Ser.,* Volume 271, pp. 1-12.

844 Sutherland, T. & Grant, J., 1998. The effect of carbohydrate production by the diatom

845 Nitzschia curvilineata on the erodibility of sediment. *Limnol. Ocenogr.,* 41(1), pp. 65-

846 72.

847   Ubertini, M. L. S., Gangnery, A., Grangere,́. K. & LeGendre, R. O. F., 2012. Spatial

848   variability of benthic-pelagic coupling in an estuary ecosystem: Consequences for

849   microphytobenthos resuspension phenomenon. *Plos One,* Volume 7.

850   Van der Biest, K. et al., 2020. Aligning biodiversity conservation and ecosystem services in

851   spatial planning: Focus on ecosystem processes. *Sci. Tot. Env.,* Volume 712, p.

852   136350.

853   van der Meer, J., 2006. An introduction to Dynamic Energy Budget (DEB) models with

854   special emphasis on parameter estimation. *J. Sea Res.,* 56(2), pp. 85-102.

855   van Ledden, M., van Kesteren, V. M. G. & Winterwerp, J. C., 2004. A conceptual framework

856   for the erosion behaviour of sand-mud mixtures. *Cont. Shelf Res.,* Volume 24, pp. 1-

857   11.

858   van Prooijen, B. C., Montserrat, F. & Herman, P. M. J., 2011. A process-based model for

859   erosion of Macoma balthica-affected mud beds. *Cont. Shelf Res.,* Volume 31, p. 527–

860   538.

861   van Prooijen, B. C. & Winterwerp, J., 2010. A stochastic formulation for erosion of cohesive

862   sediments. *J. Geophys. Res.,* 115(C01005).

863   van Rijn, L. C., 2007. Unified view of sediment transport by currents and waves. I: Initiation

864   of motion, bed roughness, and bed-load transport. *J. Hydraul. Eng.,* Volume 133, pp.

865   649-667.

866   Verdelhos, T., Marques, J. & Anastácio, P., 2015a. Behavioral and mortality responses of the

867   bivalves Scrobicularia plana and Cerastoderma edule to temperature, as indicator of

868   climate change's potential impacts. *Ecol. Ind.,* Volume 58, pp. 95-103.

869   Verdelhos, T., Marques, J. & Anastácio, P., 2015b. The impact of estuarine salinity changes

870   on the bivalves Scrobicularia plana and Cerastoderma edule, illustrated by behavioral

871   and mortality responses on a laboratory assay. *Ecol. Ind.,* Volume 52, pp. 96-104.

872 Vladimirova, I., Kleimenov, S. & Radzinskaya, L., 2003. The relation of energy metabolism

873   and body weight in bivalves (Mollusca: Bivalvia). *Biology Bull.,* 30(4), pp. 392-399.

874 Volkenborn, N., Robertson, D. & Reise, K., 2009. Sediment destabilizing and stabilizing bio-

875   engineers on tidal flats: Cascading effects of experimental exclusion. *Helgol. Mar.*

876   *Res.,* Volume 63, pp. 27-35.

877 Walles, B. et al., 2015. The ecosystem engineer Crassostrea gigas affects tidal flat

878   morphology beyond the boundary of their reef structures. *Estuaries Coast.,* Volume

879   38, pp. 941-959.

880 West, G., Brown, J. H. & Enquist, B., 1997. A general model for the origin of allometric

881   scaling laws in biology. *Science,* Volume 276, p. 122–126.

882 Widdows, J. & Brinsley, M., 2002. Impact of biotic and abiotic processes on sediment

883   dynamics and the consequences to the structure and functioning of the intertidal zone..

884   *J. Sea Res.,* 48(2), pp. 143-156.

885 Widdows, J., Brinsley, M., Salkeld, P. & Elliott, M., 1998. Use of annular flumes to

886   determine the influence of current velocity and bivalves on material flux at the

887   sediment-water interface. *Estuaries,* Volume 21, pp. 552-559.

888 Widdows, J. & Navarro, J. M., 2007. Influence of current speed on clearance rate, algal cell

889   depletion in the water column and resuspension of biodeposits of cockles

890   (Cerastoderma edule). *J. Exp. Mar. Biol. Ecol.,* 343(1), pp. 44-51.

891 Wilkes, M. A. et al., 2019. Physical and biological controls on fine sediment transport and

892   storage in rivers. *WIRES Water,* 6(2), p. e1331.

893 Willows, R., Widdows, J. & Wood, R., 1998. Influence of an infaunal bivalve on the erosion

894   of an intertidal cohesive sediment: A flume and modeling study. *Limnol. Oceanogr.,*

895   Volume 43, pp. 1332-1343.

896 Winterwerp, J. C. & van Kesteren, W., 2004. *Introduction to the physics of cohesive sediment*

897   *in the marine environment.* Amsterdam: Elsevier.

898 Winterwerp, J. C. et al., 2018. Efficient consolidation model for morphodynamic simulations

899   in Low-SPM environments. *J. Hydraul. Eng.,* 144(8), p. 04018055.

900 Wood, R. & Widdows, J., 2002. A model of sediment transport over an intertidal transect,

901   comparing the influences of biological and physical factors. *Limnol. Oceanogr.,* 47(3),

902   pp. 848-855.

903 Wrede, A. et al., 2019. Macrofaunal irrigation traits enhance predictability of nutrient fluxes

904   across the sediment-water interface. *Mar. Ecol. Prog. Ser.,* Volume 632, pp. 27-42.

905 Wrede, A. et al., 2018. Organism functional traits and ecosystem supporting services–A novel

906   approach to predict bioirrigation. *Ecol. Ind.,* Volume 91, pp. 737-743.

907 Xie, M., Simpson, S. L. & Wang, W. X., 2019. Bioturbation effects on metal release from

908   contaminated sediments are metal-dependent. *Environ. Pollut.,* Volume 250, pp. 87-

909   96.

910 Yvon-Durocher, G. et al., 2012. Reconciling the temperature dependence of respiration across

911   timescales and ecosystem types. *Nature,* Volume 487, pp. 472-473.

912 Zhou, Z. et al., 2015. Modeling sorting dynamics of cohesive and non-cohesive sediments on

913   intertidal flats under the effect of tides and wind waves. *Cont. Shelf. Res.,* Volume

914   104, pp. 76-91.

915 Zhu, Z. et al., 2016. Interactive effects between physical forces and ecosystem engineers on

916   seed burial: a case study using Spartina anglica. *Oikos,* 125(1), pp. 98-106.

917 Zwarts, L., Blomert, A., Spaak, P. & de Vries, B., 1994. Feeding radius, burying depth and

918   siphon size of Macoma balthica and Scrobicularia plana. *J. Exp. Mar. Biol. Ecol.,*

919   183(2), pp. 193-212.

920

921   **TABLES**

922   **Table 1:** Types of sediment composition. Percentages in volume of the different sediment

923   size classes (silt < 63 µm; very fine sand 63-125 µm; fine sand 125-250 µm; medium sand

924   250-500 µm; coarse sand > 500 µm) and median (D50), tenth (D10) and ninetieth percentile

925   (D90) of the sediment grain size distribution (µm).

926

Silt (%)	Very fine (%)	Fine (%)	Medium (%)	Coarse (%)	D10 (µm)	D50 (µm)	D90 (µm)
0	0	30	61	9	189	305	488
4	1	31	55	9	159	291	489
10	5	33	45	7	94	257	468
28	14	30	24	3	8	153	383

927

928   **Table 2:** Bioturbators size classes. Sediment resuspension was measured in the abiotic

929   controls and in 4 treatments with biomass equivalents (overall biomass 19 g Ash Free Dry

930   Weight m^{-2}) of differently sized bioturbators (M, mg AFDW).

931

Shell length (mm)	Body mass (M, mg AFDW)	Density of individuals (D, Ind. m^{-2})
15	36	530
20	93	247
27	247	77
35	576	33

932

933

934   **Table 3:** For each treatment with different sediment silt volume content (%) and bioturbators

935   individual body mass (M, mg AFDW), the critical flow velocity for erosion (cm sec^{-1}) were

936   estimated as the zero R_{TOT} intercept from a regression of measured R_{TOT} against V

937   (Kristensen, et al., 2013).

938

Silt (%)	M	V-Intercept	V-Slope	Critical flow velocity for erosion
0	0	-121.3	7.8	15.5
0	36	-48.6	5.7	8.5
0	93	-75.2	5.1	14.8
0	247	-53.6	6.2	8.58
0	576	-88.8	6.2	14.4
4	0	-167.8	11.1	15.2
4	36	-92.2	16.2	5.7
4	93	-70.1	14	5
4	247	-77.6	14.5	5.4
4	576	-106	11	9.6
10	0	-100.1	5.8	17.2
10	36	-108.5	9.6	11.3
10	93	-102.6	9.5	10.8
10	576	-102.2	8.1	12.6
28	0	-94.3	6.9	13.6
28	36	-103.1	9.3	11.1
28	93	-91.7	7.9	11.6
28	247	-76.3	6.4	12
28	576	-98.1	7.6	13

939

940

Table 4: Number of observations included in the ANCOVA model of the amount of suspended sediment due to bioturbation (R_{BIO}, g m^{-2}, Table 5). The initial number of 192 R_{BIO} measures (4 silt levels X 4 size levels X 6 current velocity step X 2 replicates) was reduced to 135 in way to avoid observations biased by optical disturbance to the sensor, observations related to mass erosion events and observations of decreased sediment resuspension in presence of bioturbators.

	Body mass (mg AFDW)			
Silt (%)	*36*	*93*	*247*	*576*
0	9^{b,c}	9^{b}	10^{b}	7^{b}
4	8^{d}	6^{c,d}	8^{d}	8^{d}
10	6^{d}	12^{a}	0^{e}	12^{a}
28	6^{d}	12^{a}	12^{a}	11^{c}

a: complete set of 12 measures for treatment (6 current velocity steps X 2 replicates)

b: observations missing due reduction in sediment resuspension with bioturbators

c: observations missing due to optical disturbance to the OBS sensor

d: observations missing due to mass erosion events (current velocity higher than 20 cm sec^{-1})

d: observations missing due to mass erosion events (one replicate)

e: observations missing due to mass erosion events (whole treatment)

45

956 **Table 5:** Summary of the mixed ANCOVA model of the amount of suspended sediment due

957 to bioturbation (R_{BIO}, g m^{-2}) using the silt content of the sediment as categorical explanatory

958 variable and the current velocity (V, cm sec^{-1}) and the individual mass of the bioturbators (M,

959 mg AFDW) as continuous explanatory variables. The response variable R_{BIO} and the

960 explanatory variable M were normalized *via* log transformation. A third degree polynomial

961 function of the variable V was used to account for non-linearity in the relationship between

962 current velocity and R_{BIO}. Since we took repeated measurements of the same experimental

963 units through a V gradient, we included the experimental runs as random term in the

964 ANCOVA to account for non-independence of the observations. Selection of predictive

965 variables and interaction terms was assessed by a bi-directional elimination stepwise

966 procedure. Only significant variables and interaction terms are reported in the summary table.

967 The full model (i.e. prior to variables selection) is available as an appendix (Appendix C).

|	$\log(R_{BIO})$		
Predictors	*Estimates*	*95% CI*	*p*
(Intercept)	1.47	0.23 – 2.72	0.028
log(M)	-0.42	-0.64 – -0.20	0.001
V	0.24	0.20 – 0.28	<0.001
V^3	-0.0002	-0.0002 – -0.0001	<0.001
Silt 4 %	1.01	0.34 – 1.69	0.006
Silt 10 %	0.46	-0.27 – 1.19	0.228
Silt 28 %	0.13	-0.54 – 0.80	0.702
V^3:Silt 4 %	0.0003	0.0002 – 0.0003	<0.001
V^3:Silt 10 %	0.0001	0.0001 – 0.0002	<0.001
V^3:Silt 28 %	0.0001	0.0001 – 0.0002	<0.001
Random Effects			
σ^2	0.37		
$\tau_{00\ Run}$	0.29		
ICC	0.44		
N $_{Run}$	28		
Observations	135		
Marginal R^2 / Conditional R^2	0.77 / 0.87		

968

969 **FIGURES**
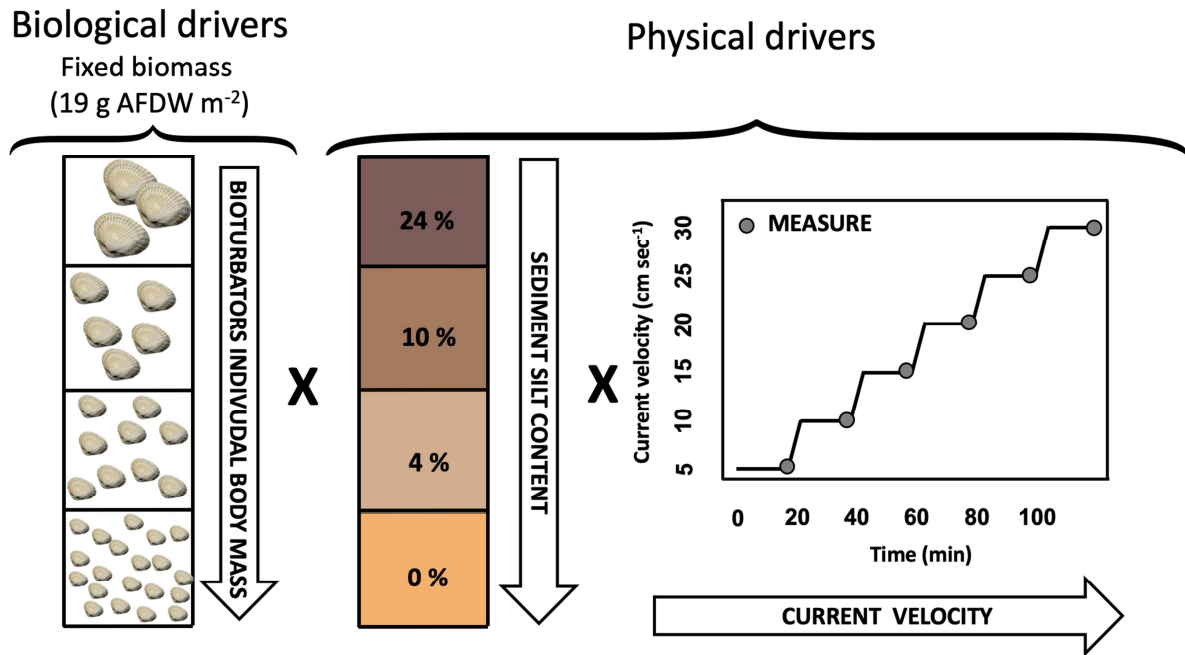
970

971 **Figure 1:** Experimental design. Keeping fixed an overall *C. edule* biomass of 19 g AFDW m$^-$

972 ^{2}, we crossed in a full factorial design 4 different size classes of individuals (36, 93, 247 and

973 576 mg AFDW of individual body mass), 4 levels of sediment silt volume content (0 %, 4 %,

974 10 % and 28 %) and 6 levels of current velocity (from 5 to 30 cm sec^{-1} by steps of 5 cm sec^{-1},

975 each step lasting 20 minutes). Each of the experimental runs with bioturbators was associated

976 to a control run using the same sediment type and current velocity gradient but without

977 bioturbators. Each experimental treatment was replicated twice.

978

47
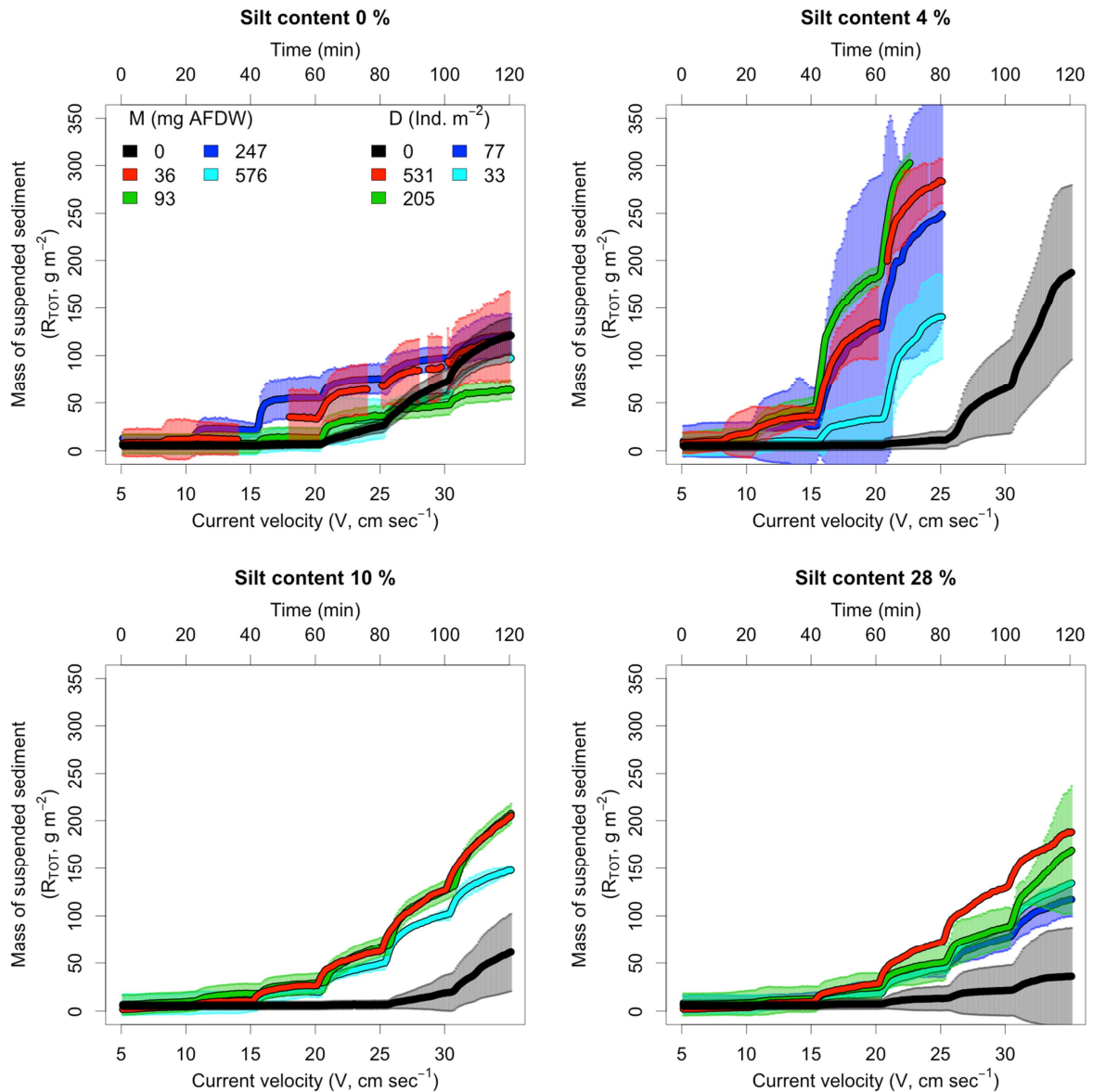
979
980 **Figure 2:** Overall mass of suspended sediment (R_{TOT}, g m^{-2}) for different sediment silt

981 volume content (%) across a gradient of current velocity (V, cm sec^{-1}) and bioturbators

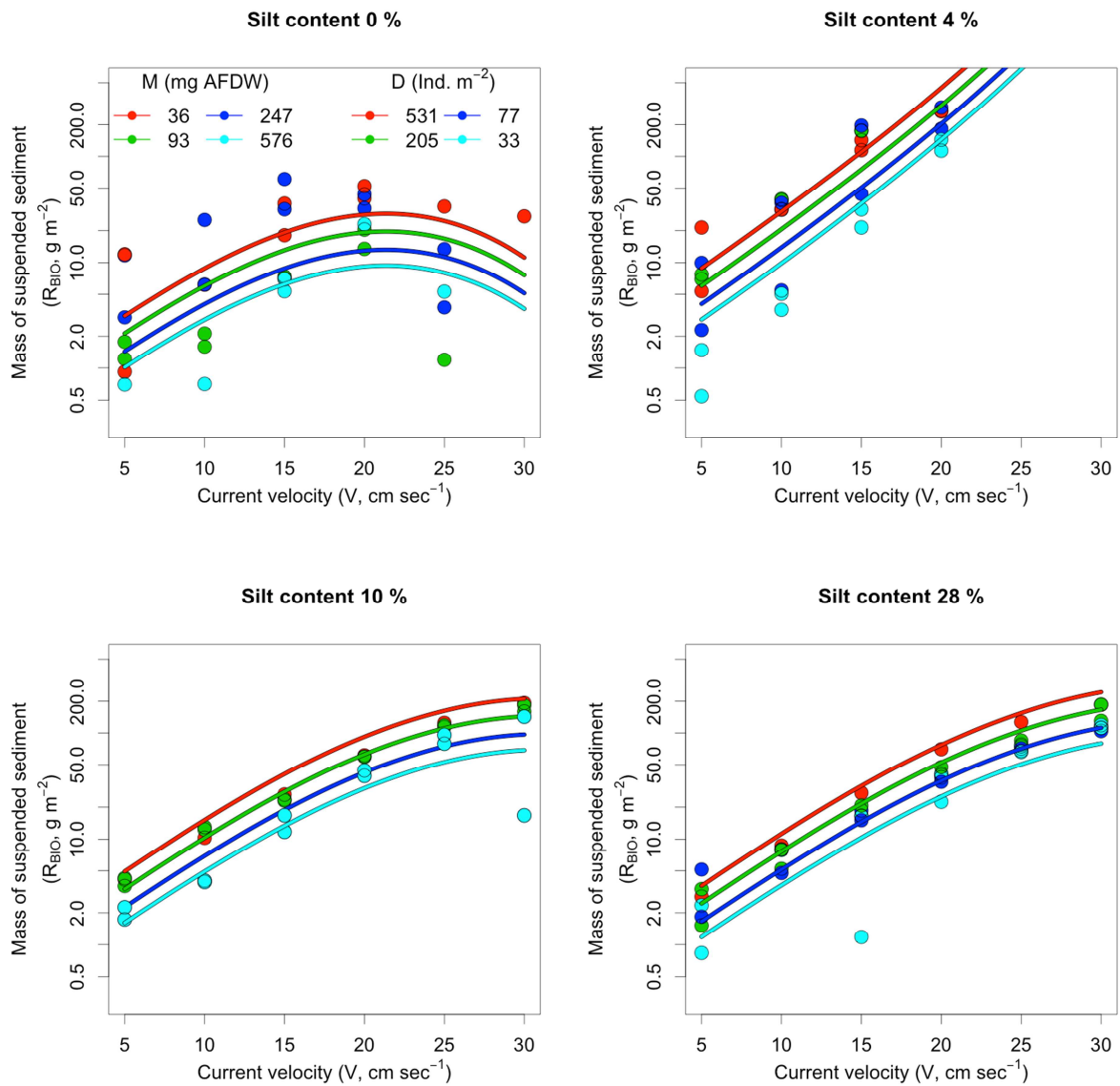982 individual body mass (M, mg AFDW, coloured lines), average of two replicates for each

983 treatment (when available). The coloured areas represent the 95 % confidence intervals
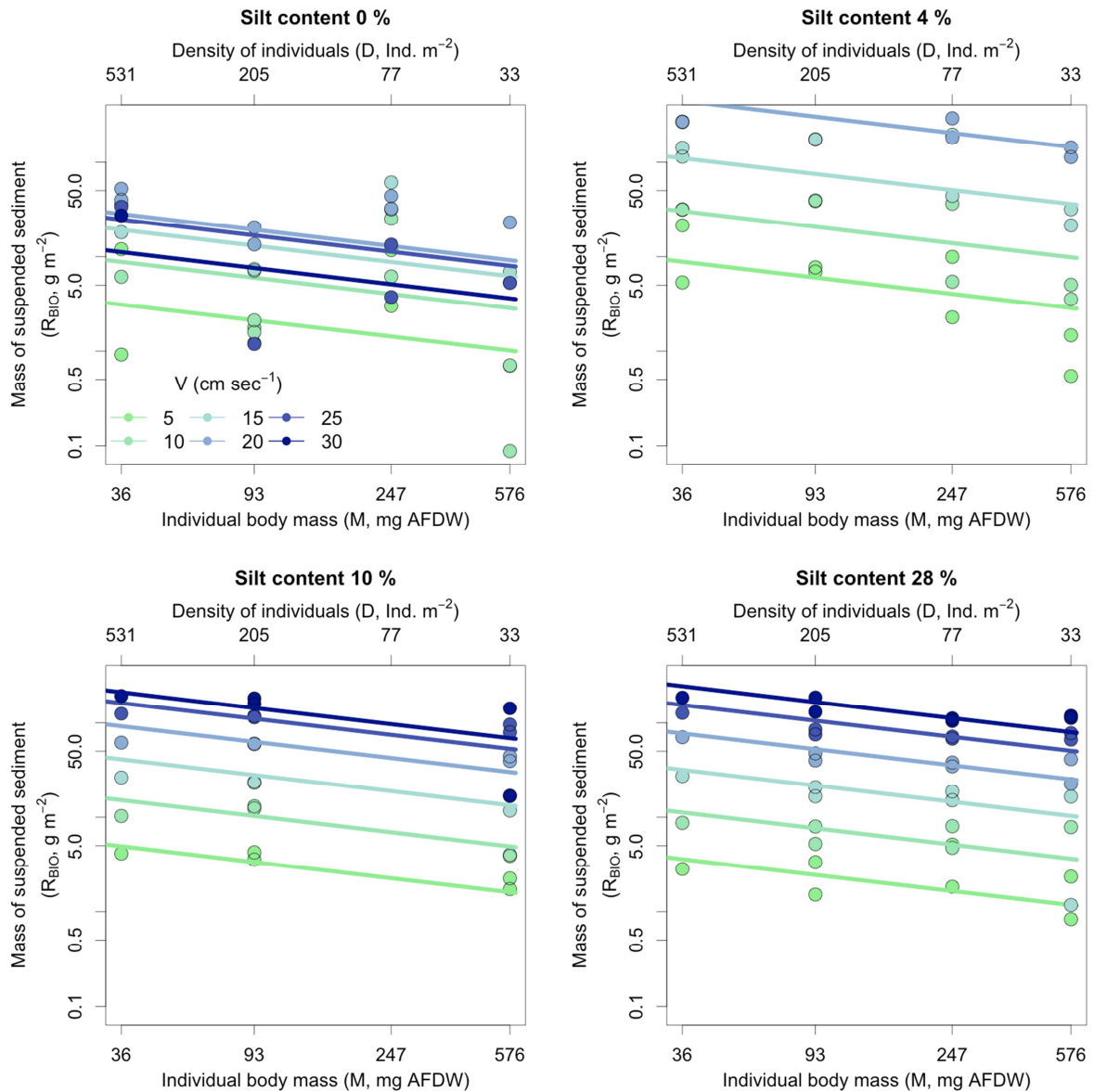
984 around the average trends.

985

Figure 3: Relationship between current velocity (V, cm sec^{-1}) and mass of suspended sediment due to bioturbation (R_{BIO}, g m^{-2}) for different sediment silt volume content (%) and bioturbators individual body mass (M, mg AFDW), as predicted from the ANCOVA model in Table 5.

49

Figure 4: Individual body mass (*M*, mg AFDW) scaling of the mass of suspended sediment due to bioturbation (R_{BIO} g m^{-2}) for different sediment silt volume content (%) and current velocities (*V*, cm sec^{-1}), as predicted from the ANCOVA model in Table 5.

Highlights:

- Bioturbators affect sediment resuspension.

- The effect of bioturbators was compared across different sediment types.

- Bioturbation effect was maximal at intermediate current and on cohesive sediment.

- The individual effect of bioturbators scales with size similarly to metabolic rate.

- The size scaling trend is independent of the sediment composition.

Declaration of interests

☐ **X** The authors declare that they have no known competing financial interests or personal relationships that could have appeared to influence the work reported in this paper.

☐The authors declare the following financial interests/personal relationships which may be considered as potential competing interests: